J|A|C|S COMMUNICATIONS

Published on Web 02/23/2010

Drastic Structural Transformation of Cadmium Chalcogenide Nanoparticles Using Chloride Ions and Surfactants

Masaki Saruyama, Masayuki Kanehara, and Toshiharu Teranishi*

Department of Chemistry, Graduate School of Pure and Applied Sciences, University of Tsukuba, 1-1-1 Tennodai, Tsukuba, Ibaraki 305-8571, Japan

Received November 9, 2009; E-mail: teranisi@chem.tsukuba.ac.jp

Semiconductor nanoparticles (NPs) have attracted great interest from fundamental and technological researchers in recent years. This is because the chemical and physical properties of NPs depend strongly on their size, shape, and crystal structure.[1] CdE (E = S, Se, Te) NPs are very attractive materials because of their size- and shape-dependent optical properties and high quantum efficiencies in the visible region. These optical properties can be applied in light-emitting diodes,[2,3] lasers,[4] nonlinear optics,[5] and biolabeling/biotagging agents.[6] For this purpose, control of the size and shape of CdE semiconductor NPs is quite important. The morphology of CdE NPs has been controlled by varying capping ligands, reactant concentration, and reaction temperature. Other approaches include photoetching,[7] surfactant-assisted etching,[8] and hydrothermal coarsening[9] of preprepared CdE NPs. However, these methods can only be used for hydrophilic NPs. Here we report a unique, facile method for the drastic structural transformation of hydrophobic CdE NPs through an Ostwald ripening process induced by Cl^- and the surfactants oleic acid (OAc) and oleylamine (OAm). We have demonstrated the versatility of this method by using it to induce structural transformations in CdSe and CdTe NPs.

For a typical structural transformation of CdS NPs, a di-*n*-octyl ether solution containing as-synthesized 3.4 ± 0.5 nm zinc blende CdS (*zb*-CdS) seed NPs[10] (Figure 1a), dimethyldistearylammonium chloride (DDAC), OAc, and OAm was heated at 260 °C for 20 min. Figure 1b shows a transmission electron microscopy (TEM) image of uniform pencil-shaped CdS NPs ("nanopencils") with widths of 17.0 ± 1.4 nm and lengths of 29.9 ± 3.3 nm formed from a solution of di-*n*-octyl ether containing CdS NPs (0.25 mmol Cd atoms), OAc (2.5 mmol), OAm (2.5 mmol), and DDAC (0.5 mmol). The uniform nanopencils tend to form vertically aligned hexagonal close-packed 2D or 3D superstructures (Figures S1 and S2 in the Supporting Information). The powder X-ray diffraction (XRD) measurements (Figure 1c) of the CdS NPs revealed that a crystal-structure transformation from *zb*-CdS seed NPs to wurtzite CdS (*w*-CdS) nanopencils took place. High-resolution TEM (HR-TEM) images of the CdS nanopencils oriented horizontally to the TEM grid (Figure 1d and Figure S3) demonstrate that the CdS nanopencils grow preferentially in the [001] direction. Almost all of the nanopencils have stacking faults near their centers, implying that stacking faults form early during growth. An HRTEM image of a CdS nanopencil taken from the [001] zone axis (Figure 1e) revealed that the side walls of the CdS nanopencils are {110} planes, which is consistent with other amine-coated hexagonal-shaped CdS nanostructures.[11] Typically, the side walls of alkylphosphonic acid-coated CdS nanorods are {100} planes.[12] This difference is derived from the atomic positions of {110} and {100} surfaces. The absorption edges of the CdS NPs red-shifted from 475 to 515 nm upon structural transformation because of the loss of an exciton confinement effect (Figure S4).

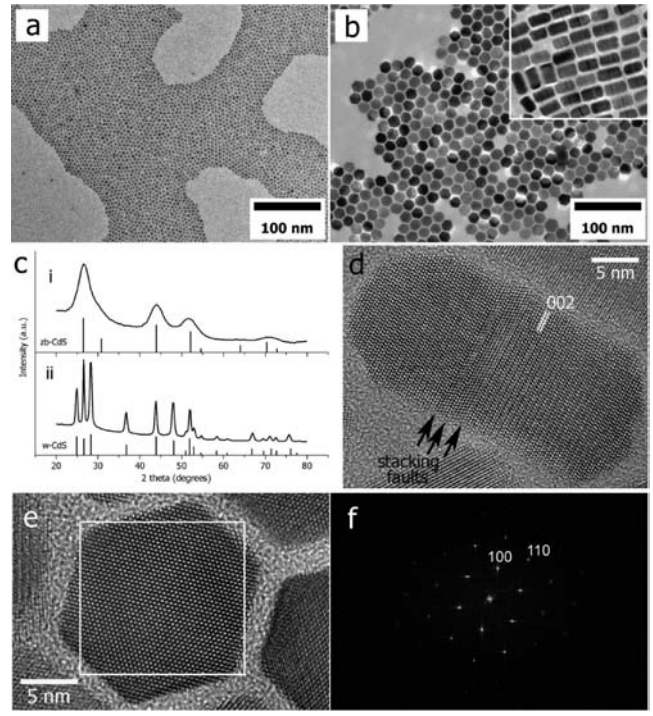

Figure 1. TEM images of (a) CdS seed NPs and (b) CdS nanopencils after reaction at 260 °C for 20 min. The inset in (b) shows a side view of the nanopencils. (c) XRD patterns of (i) CdS seed NPs and (ii) CdS nanopencils. (d) HRTEM image of a single nanopencil showing stacking faults. (e) HRTEM image of single nanopencil taken from the [001] zone axis. (f) Fast Fourier transform pattern of the rectangular region in (e).

To clarify the reaction mechanism, the NPs were microscopically monitored during the transformation reaction (Figure 2). After 3 min of reaction, the CdS NPs became polydisperse (σ = 28%) in comparison with the seed NPs (σ = 15%). Size focusing then occurred, indicating that the reaction mechanism was a typical Ostwald ripening process. An Ostwald ripening growth mechanism was observed more clearly for the transformation reaction when seed NPs with a bimodal size distribution were used.[10] Smaller CdS seed NPs (3.4 nm) dissolved early in the reaction, allowing further growth of larger seed NPs (10.5 nm) (Figure S5). This result is consistent with the Gibbs−Thompson effect, which states that smaller particles have lower dissolution temperatures because of their higher surface free energy. XRD patterns showed that the crystal-phase transformation of CdS NPs from zinc blende to thermodynamically stable wurtzite occurred at the early stage of the reaction (3 min) and was almost finished at 5 min (Figure S6). Prolonging the transformation reaction (5 h) resulted in aggregation of the CdS nanopencils (Figure S7). The morphology of an individual nanopencil in the sediment slightly changed (18.3 nm

 10.1021/ja9095285

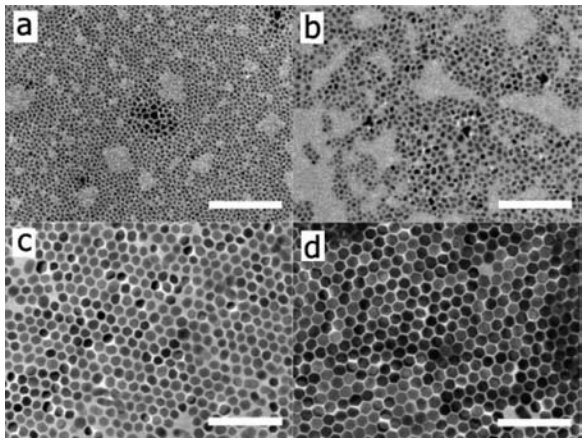

Figure 2. TEM images of CdS NPs after heating at 260 °C for (a) 1, (b) 3, (c) 5, and (d) 20 min. Scale bars represent 100 nm.

× 30.9 nm) after 20 min, which suggests that the transformation of CdS NPs was almost finished at 20 min.

To further explore the reaction mechanism, the effect of different anions on the structural transformation of the NPs was investigated. In the absence of DDAC, only a slight change in size (from 3.4 to 4.9 nm) took place through a typical Ostwald ripening process under elevated temperature[13] without changing the crystal structure, as shown in Figures S8 and S9. This indicates that DDAC plays a requisite role in the structural transformation of CdS NPs. When DDAC was replaced with HCl and the other reaction parameters were kept constant, pencil-shaped NPs with good uniformity were also obtained (Figures S8 and S9). On the other hand, when H_2SO_4 and HNO_3 were used as anion sources, only slight structural transformations of the seed NPs took place (Figures S8 and S9). The effect of halide anions on the reaction was investigated by adding different tetraoctylammonium halides (TOAX, X = Cl, Br, I) to the reaction mixture (Figure S10). Each halide anion induced significant structural transformation of the CdS NPs, although NPs with a uniform shape were formed only when TOACl was used. These experiments revealed that Cl^- is the only effective anion for the controlled structural transformation of CdS NPs. In addition, the countercation of the Cl^- source does not have a significant effect on this structural transformation.

In the Ostwald ripening process, smaller CdS NPs dissolve into ions (Cd^{2+} and S^{2-}), with Cl^- and surfactants playing a key role. For example, 3.4 nm CdS NPs were reacted with or without a combination of Cl^- and surfactants under mild conditions (100 °C). In the presence of Cl^- and surfactants, the CdS NPs gradually dissolved within 24 h (Figure S11a). No significant dissolution of the NPs was observed in the absence of Cl^- and surfactants, even after 96 h at 100 °C (Figure S11b). This result suggests that the combination of Cl^- and surfactants works to dissolve the CdS seeds, promoting the Ostwald ripening process.[14] X-ray fluorescence (XRF) analysis revealed that the white residue obtained from the dissolution of CdS NPs (Figure S12) predominantly contains Cd and Cl (Cd/Cl molar ratio ≈ 1/4) with a small amount of S. Fourier transform infrared (FTIR) analysis showed that this residue contained different chemical species depending on the Cl^- source. When HCl was used, both N−H and C−H vibration modes were detected, suggesting the presence of primary ammonium species (Figure S13). However, in the case of DDAC, the N−H vibration mode completely disappeared, suggesting the presence of quaternary ammonium species (Figure S12). These results suggest that the white residues formed when DDAC and HCl were used were $(DDA)_2CdCl_4$ and $(OAmH)_2CdCl_4$ ($OAmH^+$ = oleylammonium)

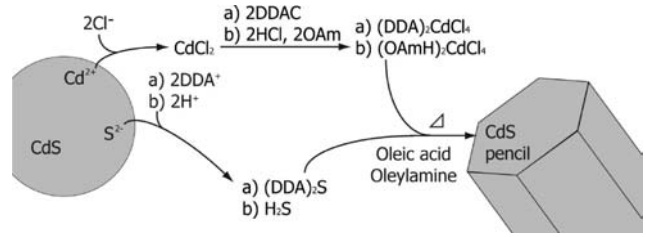

Figure 3. Schematic illustration of the proposed transformation mechanism of CdS NPs into nanopencils with (a) DDAC or (b) HCl as the Cl^- source.

complexes, respectively. These residues were found to be the precursors that form CdS nanopencils through reaction with sulfur, strongly indicating that these complexes are an intermediate species in the transformation reaction (Figure S14).

From these results, we propose the following transformation mechanism of *zb*-CdS seed NPs into nanopencils involving LCl (L = countercation of Cl^-) and surfactants (Figure 3). First, two Cl^- ions attack the Cd^{2+} ion, removing Cd^{2+} from the CdS seed NPs as $CdCl_2$. $CdCl_2$ reacts with DDAC (L = DDA^+) or OAm hydrochloride (OAm-HCl, L = $OAmH^+$) to form $(DDA)_2CdCl_4$ or $(OAmH)_2CdCl_4$, respectively. The S^{2-} ion dissolves by forming L_2S. These dissolved precursors in the solution are used in the growth of larger *w*-CdS NPs at elevated temperature. Finally, kinetically stable pencil-shaped CdS NPs are formed. Although this reaction mechanism proceeds without OAc, the resulting CdS NPs are relatively small with a broad size distribution (Figure S15), indicating that OAc is necessary for obtaining uniform CdS nanopencils during the growth stage.

On the basis of the transformation mechanism, control of the size of the CdS NPs was achieved by changing the reaction temperature and Cl/Cd molar ratio. When the reaction was conducted at 180, 200, 220, 240, and 280 °C to control the dissolution and growth rate of the NPs, CdS NPs with sizes of 5.0, 8.6, 13.3, 15.2 nm × 25.0 nm, and 20.6 nm × 31.8 nm, respectively, were obtained (Figure S16). Changing the Cl/Cd molar ratio is also an effective means of controlling the particle size, because the amount of Cl^- can vary the dissolution rate of the CdS NPs. As a result, larger amounts of Cl^- in the reaction solution gave larger NPs (Figure S17).

This Cl^- and surfactant-mediated transformation method was easily extended to other CdE NPs. Using 3.2 nm CdSe seed NPs[15] gave CdSe NPs with a pencil-shaped structure (Figure 4a−d). The size of the CdSe NPs increased as the reaction temperature increased (Figure 4b−d). Transformation of the crystal structure from *zb*-CdSe to *w*-CdSe also occurred, and the absorption edges red-shifted from 620 to 700 nm as the size of the NPs increased (Figures S18 and S19). The transformation reaction was also applied to CdTe NPs. For efficient transformation of CdTe NPs, addition of tri-*n*-octylphosphine (TOP) was required. Without TOP, the dissolution of Cd^{2+} from the CdTe seed NPs by Cl^- and the surfactants led to the precipitation of bulk Te^0 crystals because of the high reduction potential of Te^{2-},[16] resulting in a low yield of transformed CdTe. TOP molecules dissolve the bulk Te^0 crystals as TOPTe, promoting the growth of the CdTe NPs (Figure S20). The size of the NPs was readily controlled from 11 to 29 nm by changing the reaction temperature from 200 to 260 °C (Figure 4f−h), as for the CdS and CdSe systems. The transformed CdTe NPs exhibited a mixed structure of zinc blende and wurtzite with many stacking faults (Figures S21 and S22a), and the absorption edges red-shifted from 700 to 800 nm as the particle size increased (Figure S22b).

Because the resulting CdE NPs have a uniform morphology, they may act as ideal substrates for the formation of monodisperse

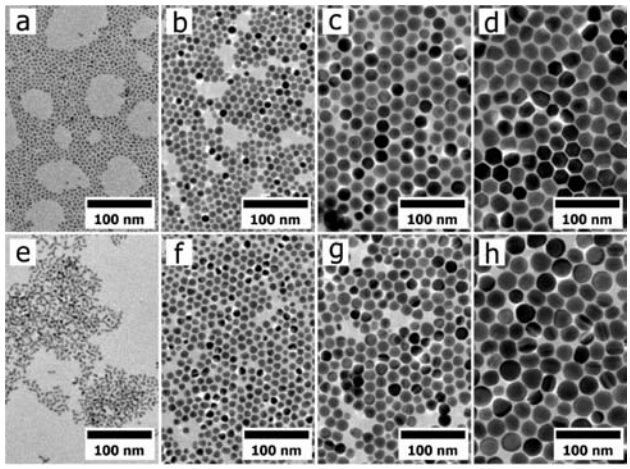

Figure 4. TEM images of (a) CdSe seed NPs (3.2 ± 0.5 nm) and CdSe NPs after reaction at (b) 240, (c) 260, and (d) 280 °C for 20 min. TEM images of (e) CdTe seed NPs (3.9 ± 0.7 nm) and CdTe NPs after reaction at (f) 200, (g) 230, and (h) 260 °C for 20 min.

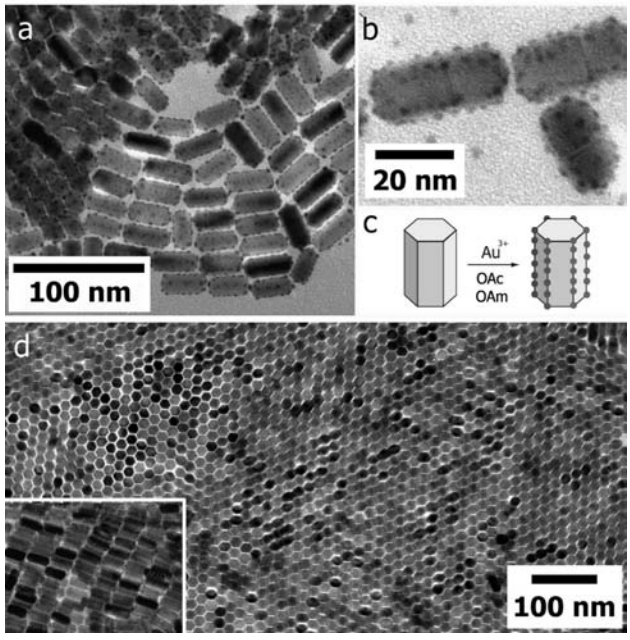

Figure 5. (a) TEM image and (b) enlarged TEM image of CdS−Au nanopencils. (c) Schematic illustration of Au deposition onto the CdS nanopencils. (d) TEM image of a CdS−Au nanopencil superlattice. The inset shows the 2D smectic array.

heterostructured NPs using a seed-mediated growth process.[17] Au can be selectively deposited on the CdS nanopencils.[10] Figure 5 shows Au NPs deposited on the CdS nanopencils to form CdS−Au nanopencils. The Au NPs selectively nucleated on the edges of the faceted CdS nanopencils because of their higher interfacial energy (Figure 5b,c). Furthermore, the morphology of the CdS nanopencils was maintained even after Au deposition, which led to superlattice formation, as observed in the seed nanopencils (Figure 5d).

In conclusion, we have developed a new general route for inducing a drastic structural transformation of hydrophobic Cd chalcogenide NPs. This reaction mechanism involves the dissolution of small NPs by Cl^- and surfactants and the subsequent growth of large NPs at elevated temperatures. In this process, Cl^- ions were required in order to generate uniform CdE NPs. These monodisperse CdE NPs are expected to be applied in areas such as photoelectronic devices. Furthermore, this transformation reaction can be readily extended for the formation of various functional materials.

Acknowledgment. We thank H. Matsumoto and T. Sato (HITACHI High-Technologies Corporation) for HRTEM measurements. This work was supported by a Grant-in-Aid for Exploratory Research (20655027) and Scientific Research on Priority Area "Strong Photon−Molecule Coupling Fields" (19049807) (T.T.) and a JSPS Research Fellowship for Young Scientists (M.S.).

Supporting Information Available: Experimental details; TEM image of superlattice of CdS nanopencils; a series of tilted TEM images, an HRTEM image, and the UV−vis absorption spectrum of CdS nanopencils; results of control experiments and experiments for CdS dissolution; TEM images of transformed CdS NPs at various temperatures and [Cl^-]; and TEM and HRTEM images, XRD patterns, and UV−vis−NIR absorption spectra of CdSe and CdTe NPs before and after the reaction. This material is available free of charge via the Internet at http://pubs.acs.org.

References

(1) (a) Ogisu, K.; Takanabe, K.; Lu, D.; Saruyama, M.; Ikeda, T.; Kanehara, M.; Teranishi, T.; Domen, K. *Bull. Chem. Soc. Jpn.* **2009**, *82*, 528. (b) Hu, J.; Li, L.-S.; Yang, W.; Manna, L.; Wang, L.-W.; Alivisatos, A. P. *Science* **2001**, *292*, 2060. (c) Yang, Y. A.; Wu, H.; Williams, K. R.; Cao, Y. C. *Angew. Chem., Int. Ed.* **2005**, *44*, 6712.
(2) Murray, C. B.; Kagan, C. R.; Bawendi, M. G. *Annu. Rev. Mater. Sci.* **2000**, *30*, 545.
(3) Alivisatos, A. P. *J. Phys. Chem.* **1996**, *100*, 13226.
(4) Klimov, V. I.; Mikhailovsky, A. A.; Xu, S.; Malko, A.; Hollingsworth, J. A.; Leatherdale, C. A.; Eisler, H.-J.; Bawendi, M. G. *Science* **2000**, *290*, 314.
(5) Ispasoiu, R. G.; Jin, Y.; Lee, J.; Papadimitrakopoulos, F.; Goodson, T., III. *Nano Lett.* **2002**, *2*, 127.
(6) Han, M.; Gao, X.; Su, J. Z.; Nie, S. *Nat. Biotechnol.* **2001**, *19*, 631.
(7) Torimoto, T.; Reyes, J. P.; Iwasaki, K.; Pal, B.; Shibuyama, T.; Sugawara, K.; Takahashi, H.; Ohtani, B. *J. Am. Chem. Soc.* **2003**, *125*, 316.
(8) (a) Akamatsu, K.; Tsuruoka, T.; Nawafune, H. *J. Am. Chem. Soc.* **2005**, *127*, 1634. (b) Li, R.; Lee, J.; Yang, B.; Horspool, D. N.; Aindow, M.; Papadimitrakopoulos, F. *J. Am. Chem. Soc.* **2005**, *127*, 2524.
(9) (a) Xiong, Y.; Zhang, J.; Huang, F.; Ren, G.; Liu, W.; Li, D.; Wang, C.; Lin, Z. *J. Phys. Chem. C* **2008**, *112*, 9229. (b) So, W. W.; Jang, J. S.; Rhee, Y. W.; Kim, K. J.; Moon, S. J. *J. Colloid Interface Sci.* **2001**, *237*, 136.
(10) See the Supporting Information.
(11) (a) Cheng, Y.; Wang, Y.; Bao, F.; Chen, D. *J. Phys. Chem. B* **2006**, *110*, 9448. (b) Chu, H.; Li, X.; Chen, G.; Zhou, W.; Zhang, Y.; Jin, Z.; Xu, J.; Li, Y. *Cryst. Growth Des.* **2005**, *5*, 1801.
(12) (a) Ahmed, S.; Ryan, K. M. *Nano Lett.* **2007**, *7*, 2480. (b) Xi, L.; Tan, X. W.; Boothroyd, C.; Lam, Y. M. *Chem. Mater.* **2008**, *20*, 5444.
(13) Thessing, J.; Qian, J.; Chen, H.; Pradhan, N.; Peng, X. *J. Am. Chem. Soc.* **2007**, *129*, 2736.
(14) Chen, Y.; Kim, M.; Lian, G.; Johnson, M. B.; Peng, X. *J. Am. Chem. Soc.* **2005**, *127*, 13331.
(15) Liu, J. H.; Fan, J. B.; Gu, Z.; Cui, J.; Xu, X. B.; Liang, Z. W.; Luo, S. L.; Zhu, M. Q. *Langmuir* **2008**, *24*, 5241.
(16) Tang, Z.; Wang, Y.; Shanbhag, S.; Giersig, M.; Kotov, N. A. *J. Am. Chem. Soc.* **2006**, *128*, 6730.
(17) (a) Teranishi, T.; Saruyama, M.; Nakaya, M.; Kanehara, M. *Angew. Chem., Int. Ed.* **2007**, *46*, 1713. (b) Teranishi, T.; Saruyama, M.; Kanehara, M. *Chem. Lett.* **2009**, *38*, 194. (c) Saruyama, M.; Kanehara, M.; Teranishi, T. *Chem. Commun.* **2009**, 2724. (d) Teranishi, T.; Saruyama, M.; Kanehara, M. *Nanoscale* **2009**, *1*, 225.

JA9095285